High Efficiency and High Rate Deposited Amorphous Silicon-Based Solar Cells

PHASE I

Annual Technical Progress Report

September 1, 2001 to August 31, 2002

NREL Subcontract No. NDJ-2-30630-08

Subcontractor: The University of Toledo

Principal Investigator: Xunming Deng
Department of Physics and Astronomy
University of Toledo, Toledo, OH 43606
(419) 530-4782
dengx@physics.utoledo.edu

Co-Investigator: Alvin D. Compaan
Victor Karpov

Contract technical monitor: Dr. Bolko von Roedern

Table of Content

Cover Page

Table of Content

List of Figures

List of Tables

Section 1 Executive Summary

Section 2 Raman and IR study of narrow bandgap a-SiGe and μc-SiGe films deposited using different hydrogen dilution

Section 3 Triple-junction a-Si Solar Cells with Heavily Doped Thin Interface Layers at the Tunnel Junctions

Section 4 High Rate Deposition of Amorphous Silicon Films Using Hot-Wire CVD With Coil-Shaped Filament

Section 5 Phase Diagram for Deposition of Amorphous and Microcrystalline Silicon

List of Figures

Figure 2-1(a) FTIR absorption spectra of a-SiGe:H films in the range from 400 to 800 cm^{-1}. The IR spectra were taken from the samples deposited under H-dilution R_H = 1.7 (GD419), 10 (GD420), 30 (GD422), 50 (GD423), 120 (GD424), 180 (GD449) and 240 (GD450), respectively

Figure 2-1(b) FTIR absorption spectra of a-SiGe:H films in the range from 1800 to 2200 cm^{-1} (b). The IR spectra were taken from the same samples as in Figure 2-1(a).

Figure 2-2 The relative intensity I_{2090} and hydrogen content C_H of a-SiGe:H samples as a function of H-dilution R_H .

Figure 2-3 Raman spectra of high H-dilution a-SiGe:H samples, with R_H=120 (GD424), 180 (GD449) and 240 (GD450), respectively. The Raman spectra were taken from the front surface of the samples, except GD450R, which was taken from the back side of sample GD450 through the glass substrate.

Figure 3-1 IV curve of a UT fabricated triple cell, showing 12.7% initial, active-area efficiency.

Figure 3-2 Quantum efficiency curve of 12.7% cell (GD585) showing the QE for top, middle and bottom cells. The figure also shows the short circuit current under UT simulator and AM1.5 spectrum.

Figure 3-3 IV curve of GD585 measured at NREL, showing 11.8% initial, total-area efficiency.

Figure 3-4. I-V curve of a triple cell showing 10.7% stable efficiency.

Figure 4-1 Schematic diagram of the Hot Wire CVD deposition chamber.

Figure 5-1. Calibration of actual substrate temperature from the reading temperature for UT's PECVD deposition system.

Figure 5-2 Voc of nip solar cells as a function of hydrogen dilution for different substrate temperatures

Figure 5-3 Contour plot of the Voc as a function of substrate temperature and H dilution

Figure 5-4 Phase diagram for the a-Si and microcrystalline growth in Ts-R plot.

List of Tables

Table 2-1 Performance of a SiGe:H n-i-p devices made with different H dilution $R_{H.}$

Table 3-1 I-V performance of triple cell having heavily doped tunnel-junction interface layers with different thicknesses

Table 3-2 IV performance of top, middle and bottom component cells before and after 1000 hours of light soaking with 1 sun intensity at 50 ^{o}C.

Table 3-3 IV performance for triple-junction a-Si based solar cells measured at UT and NREL.

Table 4-1. Deposition conditions of a-Si:H films using HWCVD. All samples were deposited at 100 mTorr with a filament temperature of 2000 °C.

Table 4-2. Properties of a-Si:H films deposited using HWCVD.

Table 5-1 Single-junction a-Si solar cell devices fabricated to map out the deposition phase diagram in terms of substrate temperature and hydrogen dilution

Table 5-2 Thickness of the nip layers for the 42 samples fabricated to map out the phase diagram. The thickness shown is in nm.

Table 5-3 Growth rate, in A/s, of i-layers deposited under different conditions.

Table 5-4 Open circuit voltage of the 42 samples fabricated to map out the phase diagram

Section 1 Executive Summary

This report covers the first year of this subcontract for research on High Efficiency and High-Rate Deposited Amorphous Silicon-Based Solar Cells, under subcontract number NDJ-1-30630-08. The period of performance covered by this report is September 1, 2001 to August 31, 2002.

Following this Executive Summary are four sections performed during each of the four quarters. The subject of these four sections are:

- Section 2 Raman and IR study of narrow bandgap a-SiGe and μc-SiGe films deposited using different hydrogen dilution

- Section 3 Triple-junction a-Si Solar Cells with Heavily Doped Thin Interface Layers at the Tunnel Junctions

- Section 4 High Rate Deposition of Amorphous Silicon Films Using Hot-Wire CVD With Coil-Shaped Filament

- Section 5 Phase Diagram for Deposition of Amorphous and Microcrystalline Silicon

In the following, we summarize the activities related to each of the seven tasks under this subcontract.

Task 1: Grand phase diagram for deposition of protocrystalline Si and SiGe materials.

Under this task, we studied the phase diagram for a-Si deposition for different H dilution and substrate temperature Ts. We found that the transition from amorphous to microcrystalline occurs with lower hydrogen dilution R at Ts~200C. At higher and lower Ts, higher R is needed to deposit microcrystalline. The results are summarized in Section 5. We are in the process of constructing a new addition to our PECVD deposition system. The new addition, with three new sputter deposition targets for Al, ZnO and ITO sputtering, will be integrated into the PECVD system. The load chamber for this system wil be able to have multiple substrate carrier with different masks. This would allow us to do the combinatorial design and accumulate large amount of data to construct an extensive phase diagram.

Task 2: Deposition of a-Si based materials using new gas precursors

This task is performed together with Voltaix, Inc., which supplies trisilane gas for deposition of a-Si based materials. Trisilane gas cylinder has been produced and installed in UT's deposition system. We have carried out extensive system calibration so that a comparative study between trisilane and disilane can be performed. Detailed results on the trisilane study will be reported in a quarterly report during the Second Year.

Task 3: Study of nanometer-sized doped layers and the band-edge mismatch at hetero-interfaces

Extensive research is carried out in this area. We studied extensively two interfaces: 1) the p-i interface and 2) the p-n interface at the tunnel junctions. The study on p-i interface for a-Si and a-SiGe solar cells is reported in the 29th IEEE Photovoltaic Specialist Conference, held in May, 2002. The paper is not attached in this report but can be obtained from the Proceedings of IEEE PVSC. In summary, we found that the p-layer optimized for a-Si top cell causes severe J-V roll-over when it is used for narrow bandgap a-SiGe alloys. We conclude that the band mismatch at the p-i interface prevents holes from being collected at the p-layer under a forward bias near Voc point (when the field is weakened). This causes reduced carrier injection, and consequently the poor roll-over behavior in the J-V characteristics.

The study on the p-n interface at the tunnel junction is summarized in Section 3.

Task 4: Fabrication of triple-junction cells

Thirty six triple-junction solar cells were fabricated during this program period to improve efficiency of triple-junction solar cells. Many of these solar cells show initial, active-area efficiency exceeding 12%. The stabilized efficiency is around 10.5-11%. The research on triple-junction solar cells is highlighted in Section 3.

Task 5: Technique for measuring component cell I-V in a two-terminal triple stack

The research activities in this area consists of two parts: 1) the experimental work has been mostly focused on two-junction, two-terminal device. The study was carried out using UT's quantum efficiency system. The component cell performance in a tandem structure was measured using various bias light conditions. Further systematic study is still needed to demonstrate satisfactory results; 2) In addition to the experimental work, we have established a procedure that is expected to allow us to measure the J-V of component cells in a triple-junction stack. Experimental work needs to be performed to verify the effectiveness of the developed procedures.

Task 6: Modeling of triple-junction cells with AMPS and comparison with fabricated devices.

We have performed modeling work in conjunction with the fabrication of triple cells. So far, the modeling effort has not been successful in terms of providing directions and guidelines to the device optimization. Modeling research has been performed on single-junction solar cells to study the interface behavior. The results was reported in the 29th IEEE PVSC, May, 2002.

Task 7: High-rate deposition of a-Si based solar cells

We have conducted extensive research using a hot-wire CVD process with a coiled filament and multiple gas inlets. Two papers were presented in the 2nd International Conference on Cat-CVD. Using such a coiled filament, we deposited a-Si films at a deposition rate up to 240 A/s. These films show a low microstrcture R* (around or less than 0.1). At a low Ts and without H dilution, we deposited a-Si films at a rate up to 800 A/s. Unfortunately, these 800-A/s deposited films are porous and with its H mostly in dihydride form, as revealed from FTIR.

Section 2 Raman and IR study of narrow bandgap a-SiGe and μc-SiGe films deposited using different hydrogen dilution

Contributors: X. Liao, W. Wang and X. Deng

Summary

Hydrogenated amorphous silicon-germanium (a-SiGe:H) films and n-i-p solar cells near the threshold of microcrystalline formation have been prepared by plasma enhanced chemical vapor deposition (PECVD) with a fixed germane to disilane ratio of 0.72 and a wide range of hydrogen dilution R_H=(H_2 flow)/(GeH_4+Si_2H_6 flow) values of 1.7, 10, 30, 50, 120, 180 and 240. The effects of R_H on the structural properties of the films were investigated using Raman scattering and Fourier transform infrared (FTIR) absorption spectroscopy. It is found that H dilution causes the H content, especially that in SiH_2 configuration, in a-SiGe:H films to decrease and finally leads the films through amorphous to microcrystalline transition. The onset of the phase transition occurs at R_H about 180, and the crystalline formation begins first in the Si-rich region. Light soaking tests on the solar cells demonstrate that the devices with higher R_H exhibit higher stabilized efficiency after 1000 hours of 1 sun light soaking.

1. Introduction

Narrow band gap a-SiGe:H alloy has attracted a great deal of attention for application in the tandem and triple-junction solar cells, because its optical band gap can be tailored by changing the Ge content to match longer wavelengths of the solar spectrum. However, as the Ge content increases and the bandgap decreases, the electronic and structural properties of the films tend to be inferior. Although in recent years the defect density in a-SiGe:H films has been much suppressed by e.g. H-dilution [1], cathode deposition [2], and using disilane-germane mixture without H dilution [3] in PECVD process, the further improvement in the film quality has been a challenging issue in the research and development of a-Si:H based solar cells. In the previous reports we performed a systematic investigation of the effects of Ge content [4] and H dilution [5] on the electrical and optical properties of a-SiGe:H films. In this paper we report the impact of H dilution on the structural properties of a-SiGe:H films and n-i-p solar cells near and above the threshold of crystallinity.

2. Experimental

The a-SiGe:H films, approximately 0.5 μm thick, were deposited on 7059 glass, crystalline silicon (c-Si) wafer and stainless steel (SS) substrates using rf (13.56 MHz) PECVD in a ultrahigh-vacuum, multi-chamber, load-locked deposition system. A gas mixture of disilane, germane and hydrogen was used with a fixed germane to disilane ratio of 0.72 and a varying hydrogen dilution ratio R_H of 1.7, 10, 30, 50, 120, 180 and 240, which is defined as the ratio of gas flows of [H_2] to [Si_2H_6] + [GeH_4]. The germane to disilane ratio is the same as what we typically use for the i-layer in the narrow-bandgap bottom cell of our standard triple-junction solar cells [6]. FTIR absorption measurements were taken for samples on c-Si substrates to obtain information on the H content and bondings. In order to analyze the structural properties, Raman scattering spectra were recorded from the films on 7059 glass and n-i-p cell devices on stainless steel, upon the excitation of an argon laser with 488nm wavelength.

Single junction n-i-p solar cells using these a-SiGe materials as the i-layers were deposited on SS substrates without the use of a back-reflector. I-V measurements were taken under a Xe-lamp solar simulator under AM1.5 spectrum. Light soaking was performed under one-sun light intensity using a metal halide lamp. The light intensity is maintained at such a level that a reference Si solar cell generates the same current as it does under a Xe-lamp simulator.

3. Results and Discussions

3.1 FTIR absorption spectra

The FTIR absorption spectra of seven a-SiGe:H samples are plotted in figures 1(a) and 1(b) with a varying H-dilution $R_H = 1.7$ (GD419), 10 (GD420), 30 (GD422), 50 (GD423), 120 (GD424), 180 (GD449) and 240 (GD450), respectively. The arrangement of the spectra in these figures is in the sequence from top to bottom with R_H increasing. Figure 2-1(a) shows the IR spectra ranging from 400 to 800 cm^{-1}. It is seen from this figure that a prominent peak appears at about 560-640 cm^{-1} region, which is assigned to the bending vibration of Si-H and Ge-H bonds. As R_H decreases from 1.7 to 240, the peak intensity is monotonically decreased, indicating that the hydrogen content (C_H) in the films descends with increasing H dilution, while its peak position is not obviously affected. However this peak position has a small red shift, due to the existence of Ge-H bonds in the a-SiGe:H films, in respect to the bending mode of Si-H bonds in a-Si:H at 640 cm^{-1}. This is similar to the earlier results in the literature [7], that reported the wagging or rocking modes of Si-H bonds gradually shifting from 640 cm^{-1} to 560 cm^{-1}, as the Ge relative content increased from 0 to 1.

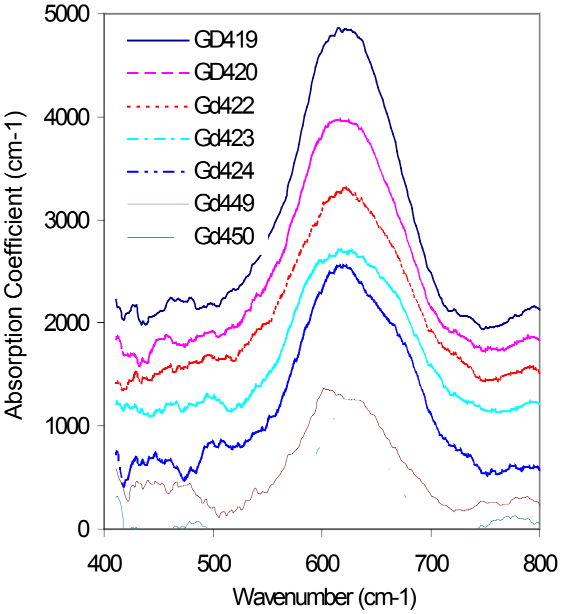

Figure 2-1(a) FTIR absorption spectra of a-SiGe:H films in the range from 400 to 800 cm^{-1}. The IR spectra were taken from the samples deposited under H-dilution $R_H = 1.7$ (GD419), 10 (GD420), 30 (GD422), 50 (GD423), 120 (GD424), 180 (GD449) and 240 (GD450), respectively

Figure 1(b) shows the IR spectra ranging from 1800 to 2200 cm^{-1}. It is seen that a few absorption features appear at about 2090, 2000 and 1872 cm^{-1}, which are respectively assigned to stretching vibrations of SiH_2, SiH and GeH configurations.

It is interesting to note the impact of R_H on the relative intensity of the stretching mode at 2090 cm^{-1}, I_{2090}, which is defined as the ratio of its intensity to that of the peak at 2000 cm^{-1}. As R_H increasing from 1.7 to 120, the relative intensity I_{2090} becomes weaker. This suggests that the relative concentration of SiH_2 configuration in a-SiGe:H films decreases with R_H increasing. But as R_H further increasing from 120 to 240, the relative intensity I_{2090} starts to increase. The dependence of I_{2090} on R_H could be seen more clearly in Figure 2-2. This enhancement of I_{2090} at higher R_H is likely correlated with the formation of the microcrystalline phase in the films. We assigned it to H_2* complexes in the boundaries between microcrystallites [8].

The influences of H-dilution on the hydrogen content C_H is also illustrated in Fig.2, which was derived from the IR absorption coefficient of the Si-H bending mode in Figure 2-1(a). It shows that C_H decreases as R_H increases, except one point corresponding to the phase transition region R_H=120, where an anomalous increase in C_H was found. This is similar to the observation in a-Si:H when deposited under high H-dilution to the phase transition region [9].

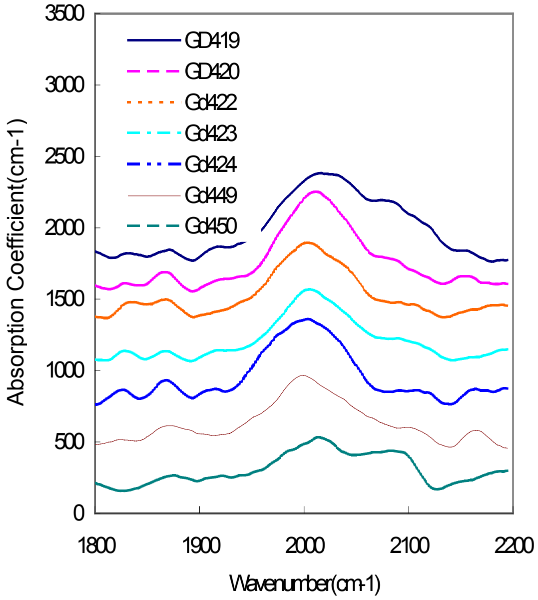

Figure 2-1(b) FTIR absorption spectra of a-SiGe:H films in the range from 1800 to 2200 cm^{-1} (b). The IR spectra were taken from the same samples as in Figure 2-1(a).

3.2 Raman spectra

To clarify the structural variation we performed Raman spectroscopy measurements on the three highest diluted samples. Figure 2-3 shows the Raman spectra taken from the front surface of the a-SiGe:H samples deposited on 7059 glass under R_H=120 (GD424), 180 (GD449) and 240 (GD450), respectively. For comparison the Raman spectrum of GD450R taken from the back-side of the sample of GD450 through the glass substrate is also shown in the figure.

It is seen that for the sample of GD424 (R_H = 120) two broad envelops were observed at ~394 and ~260 cm^{-1}, which may correspond to Si-Ge and Ge-Ge vibrations in the amorphous network. In addition, a shoulder at ~476 cm^{-1} was recognized, which should correspond to the TO phonon of a-Si. These results are similar to the earlier report on Raman spectra of a-SiGe:H [7].

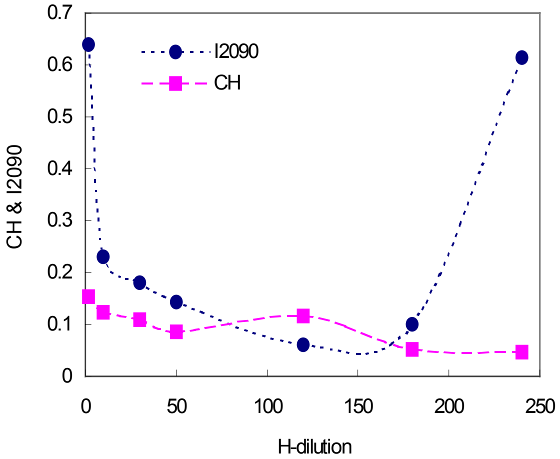

Figure 2-2 The relative intensity I_{2090} and hydrogen content C_H of a-SiGe:H samples as a function of H-dilution R_H .

For the sample of GD450, it can be seen clearly that a few crystalline SiGe Raman characteristic peaks appear in the spectrum, including the Si-Si TO phonon at 496cm^{-1}, the Si-Ge vibration at 402cm^{-1} and Ge-Ge TO phonon at 284cm^{-1}. It notes that the Si-Si TO phonon has a red-shift, compared with the c-Si TO phonon. The lowered frequency could be explained in terms of the presence of the larger mass neighboring Ge atoms in the network. These observations are similar to the results reported by Jelenkovic et al [10], who obtained the similar three Raman peaks from the SiGe samples prepared by rf magnetron sputtering followed by a post-annealing crystallization at 550°C.

For Sample GD449, with a little lower H-dilution R=180 than GD450, we find that it locates near the phase transition region from amorphous to microcrystalline state. The crystalline characteristic Si-Si vibration at 498cm^{-1} is just beginning to appear in the Raman spectrum, while the Si-Ge vibration at 394 cm^{-1} keeps nearly unchanged, compared to its amorphous counterpart. The similar situation was also observed in the literature [10], where the crystalline Si-Si Raman peak first appeared in their spectra and then grew in intensity with the post-annealing time (see their Fig.4). It seems that there are phase segregation phenomena occurring in a-SiGe:H films and the crystallization is beginning first from the Si-rich region in the films.

For the Raman spectrum GD450R, taken from the back-side of GD450 through the glass substrate, only one broad peak can be found at 480cm^{-1}, indicating that the film first grown on the glass substrate is still in amorphous state, even though R_H is as high as 240. Crystallization in a-SiGe:H films is thickness-dependent as observed in a-Si:H[11].

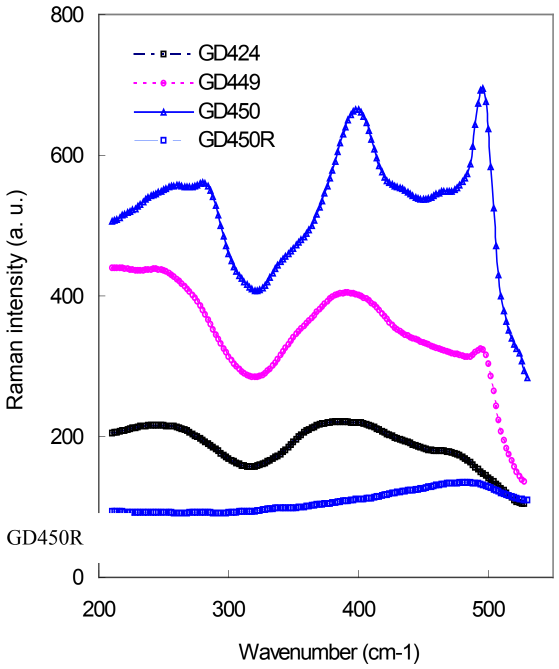

Figure 2-3 Raman spectra of high H-dilution a-SiGe:H samples, with R_H=120 (GD424), 180 (GD449) and 240 (GD450), respectively. The Raman spectra were taken from the front surface of the samples, except GD450R, which was taken from the back side of sample GD450 through the glass substrate.

3.3 a-SiGe:H n-i-p solar cells

The structural variation in a-SiGe:H intrinsic layer with H-dilution should be reflected in the performances of constituent solar cells. Table 2-1 lists the photovoltaic parameters of a-SiGe:H n-i-p devices made with different H dilution R_H [5]. It is seen from the Table that the short circuit current density J_{sc} is roughly unchanged within the experimental error. The fill factor FF seems to increase with H-dilution, but with some fluctuation. The open circuit voltage V_{oc} increases from 0.64 V to 0.67 V with R_H up to 120, before it starts to decrease down to 0.64 V when R_H is further increased to 240. This may be correlated with the fact that small amount of microcrystalline phase is formed at R=240.

Considering the fact that the a-SiGe n-i-p solar cells are deposited on stainless steel and only about 170nm thick, we also performed Raman scattering measurements on the solar cells. For the sample GD451 with intrinsic layer deposited under R_H=180, the obtained Raman spectrum shows a main peak at ~480 cm^{-1} and a small shoulder at ~ 500cm-1, which could be respectively assigned to the Si-Si TO phonon in amorphous and crystalline network. This verifies that the sample is indeed at the beginning of the phase transition from amorphous to crystalline state.

Light soaking tests for these a-SiGe:H samples were also performed to understand the effect of R_H on the device stability. The last column of Table 2-1 shows the degradation under one-sun light soaking at 50 ^oC for 1000 hours. It is found that the degradation is reduced with higher R_H, down from 21% for R_H =10 to 11% for R=120.

Table 1 Performance of a SiGe:H n-i-p devices made with different H dilution $R_{H.}$

Device	H dilut	V_{oc}	J_{sc}	FF	Eff	Light Degrad.
No.	R_H	(V)	(mA/cm^2)	(%)	(%)	(%)
GD429	1.7	0.638	16.2	53.8	5.54	
GD428	10	0.64	17.7	53.1	6.02	20.9
GD425	30	0.656	17.4	59.1	6.76	21.6
Gd426	50	0.662	17.2	55	6.25	14.2
GD427	120	0.669	17	54.8	6.25	11.4
GD451	180	0.656	18.1	56	6.65	--
GD452	240	0.636	18.5	55.8	6.55	--

4. Conclusion

We have deposited a series single-layer films and n-i-p solar cells using narrow bandgap a-SiGe:H materials deposited via PECVD using different H-dilution ranging from R_H=1.7 to 240. Samples with higher R_H value showed lower amounts of H incorporated into the films, especially in the SiH_2 configuration, and exhibited higher light soaking stability. The onset of the phase transition from a-SiGe:H to μc-SiGe:H occurs at about R_H=180. The results from the films and devices deposited using different H-dilution suggest that high H dilution up to 120 could be used to deposit a-SiGe:H films and devices with improved light stability.

References

[1] J. Yang, A. Banerjee, T. Glatfelter, K. Hoffman, X. Xu and S. Guha, "Correlation of component cells with high efficiency amorphous silicon alloy triple junction solar cells and modules", Proc. 1st world Conf. on Photovoltaic Energy Convention (Waikoloa, 1994) pp. 387-390.

[2] P. Wickboldt, D. Pan, W. Paul, J. H. Chen, F. Zhong, J. D. Cohen, Y Chen and D. L. Williamson, "Improved a-$SiGe_{1-x}Ge_x$:H of large x deposited by PECVD", J. Non-Cryst. Solids, 198-200, 1996, pp. 567-571.

[3] A.Matsuda and G. Ganguly, “Improvement of hydrogenated amorphous silicon germanium alloys using low power disilane–germane discharges without hydrogen dilution”, Appl. Phys. Lett., 67, 1995 pp. 1274-1276.

[4] P. Agarwal, H. Povolny, S. Han and X. Deng, “Study of a-SiGe:H Films and n-i-p Devices used in High Efficiency Triple Junction Solar Cells”, J. of Non-Cryst. Solids, 299-302, 2002 pp. 1213-1218.

[5] H. Povolny, P. Agarwal, S. Han and X. Deng, “Comparison Study of a-SiGe Solar Cells and Materials Deposited Using Different Hydrogen Dilution”, Mat. Res. Soc. Symp. Proc. 609, 2000, A30.3.

[6] X. Deng and X.B. Liao, S. Han, H. Povolny and P. Agarwal, “Amorphous Silicon and Silicon Germanium Materials for High Efficiency Triple-junction Solar Cells”, Solar Energy Materials & Solar Cells, 62, 2000, pp. 89-95.

[7] Y. Chou and S. Lee, “Structural, optical, and electrical properties of hydrogenated amorphous silicon germanium alloys”, J. Appl. Phys. 83, 1998, pp. 4111-4123.

[8] S. Sheng, X. Liao and G. Kong, “Study of the microstructure of high stability a-Si:H films by Raman Scattering and infrared absorption spectra”, Appl. Phys. Lett., 73, 1998, pp. 336-338.

[9] U. Kroll, J. Meier, A. Shah, S. Mikhailov and J. Weber, “Hydrogen in amorphous and microcrystalline silicon films prepared by hydrogen dilution”, J. Appl. Phys., 80, 1996, pp. 4971-4975.

[10] E. V.Jelenkovic, K.Y. Tong, Z. Son, C. L. .Mak, and W.Y. Cheung, “Properties of crystallized $Si_{1-x}Ge_x$ thin films deposited by Sputtering”, J. Vac. Sci. Technol. A 15, 1997 pp. 2836-2841.

[11] R. J. Koval et al., “Performance and stability of Si:H p-i-n solar cells with i layers prepared at the thickness-dependent amorphous-to-microcrystalline phase boundary”, Appl. Phys . Lett. 75, 1999, pp. 1553-1555.

Section 3 Triple-Junction a-Si Solar Cells With Heavily Doped Thin Interface Layers At The Tunnel Junctions

Contributors: W. Wang, H. Povolny, W. Du, X.B. Liao and X. Deng

ABSTRACT

Triple-junction a-Si based solar cells, having a structure of SS/Ag/ZnO/n^+/n/b/a-SiGe-i/b/p/p^+/n^+/n/b/a-SiGe-i/b/p/p^+/n^+/n/a-Si-i/p/p^+/ITO, are fabricated at the University of Toledo using a multi-chamber, load-locked PECVD system. We studied the effect of heavily doped p^+ and n^+ layers deposited at the tunnel junction interfaces between the top and middle component cells and between the middle and bottom component cells on the efficiency of triple-junction solar cells. Preliminary results show that thin, ~ 1nm, interface p^+/n^+ layers improve the solar cell efficiency while thicker interface layers, ~4nm thick, cause the efficiency to decrease. Incorporating the improved interface layers at the tunnel junctions, as well as earlier improvements in the intrinsic layers, the p-i interface in terms of reducing the band-edge offset, and the a-SiGe component cells using bandgap-graded buffer layers, we fabricated triple-junction solar cells with 12.71% efficiency in the initial state and 10.7% stable efficiency after 1000 hours of 1-sun light soaking. Samples sent to NREL for independent measurements show 11.8% total-area (or 12.5% active-area) initial efficiency.

INTRODUCTION

Triple-junction solar cell structure have been studied and used extensively to deposit high-efficiency a-Si based solar cells. Using a triple cell structure, United Solar Systems Corp. fabricated a-Si/a-SiGe/a-SiGe solar cells with 13% stabilized efficiency [1]. In such a triple-junction, two-terminal structure, the tunnel junction between the doped layers of neighboring component cells are formed due to the high concentration of recombination centers from the dangling bond defects in the doped a-Si materials. For this reason, the doped layers at the tunnel junctions are usually made thicker and/or with higher doping concentrations than those for single-junction solar cells [2]. However, a thicker doped layer would result in an optical loss and a higher doping concentration would result in a reduced bandgap, consequently, a lower Voc. In an earlier work [3], doping graded p-layer was studied in an n-i-p-n test structure. It was found that a p-layer with higher doping near the n-layer and lower doping near the i-layer leads to improved efficiency compared with a p-layer with constant doping [3]. In this work, we investigate the impact of inserting heavily doped thin interface layers at the tunnel junction to enhance the recombination of carriers from neighboring component cells.

EXPERIMENTAL

The structure of triple-junction a-Si based solar cell fabricated in this study is SS/Ag/ZnO/n^+/n/b/a-SiGe-i/b/p/p^+/n^+/n/b/a-SiGe-i/b/p/p^+/n^+/n/a-Si-i/p/p^+/ITO, where SS is stainless steel foil substrate, p^+ and n^+ are heavily doped interface layers, and /b/ on both sides of a-SiGe i-layers are bandgap graded buffer layers. All of the semiconductor layers were deposited using University of Toledo (UT)'s multiple-chamber PECVD system. The substrate coated SS is provided by Energy Conversion Devices, Inc. (ECD) and United Solar. ITO is deposited at UT using rf sputtering from a ITO target in Ar ambient. The solar cells were characterized at UT using a Xe-lamp solar simulator and a quantum efficiency measurement system with optical and electrical bias capability, allowing us to measure the QE of component cells in a triple-junction two-terminal stack. Detailed description of the experimental details can be found in our earlier reports [4].

RESULTS AND DISCUSSIONS

Heavily doped p^+ and n^+ interface layer at the tunnel junctions

Table 3-1 shows the I-V characteristics of a series of four triple-junction solar cells having a structure SS/Ag/ZnO/n_1^+/n_1/b/a-SiGe-i_1/b/p_1/p_1^+/n_2^+/n_2/b/a-SiGe-i_2/b/p_2/p_2^+/n_3^+/n_3/a-Si-i_3/p_3/p_3^+/ITO, where p_1^+/n_2^+ and p_2^+/n_3^+ interface layers are varied while all other layers are essentially kept unchanged for the set of devices. These heavily doped layers were deposited using a doping ratio of BF_3:SiH_4=1.7:1 for the p^+ layer and PH_3: SiH_4=1:10 for the n^+ layer. The deposition rates for the p^+ and n^+ layers are estimated to be 0.3 Å/s and 1 Å /s, respectively.

Table 3-1 I-V performance of triple cell having heavily doped tunnel-junction interface layers with different thicknesses

p^+ and n^+ interface layer deposition time (s)		Voc (V)	Jsc (mA/cm^2)	FF (%)	η (%)	Device Number
p_1^+ & p_2^+	n_2^+ & n_3^+					
0	0	2.300	7.25	68.4	11.4	GD846
10	10	2.314	7.54	69.2	12.1	GD840
20	20	2.276	7.55	69.7	11.9	GD842
40	40	2.222	7.02	66.3	10.4	GD854

As we see from the Table, GD846 was fabricated without heavily doped interface layer and is used here as a reference sample. Compared with GD846, GD840 (made with 10 s p^+/n^+ layers) show an improvement in both the J_{sc} and FF. More devices will be fabricated to confirm that there is indeed an improvement in the current when thin p^+/n^+ layers are inserted at the tunnel junctions. The loss of current in GD846, if further confirmed, would likely be due to an insufficient amount of recombination centers near the tunnel-junction interface, hindering photo-generated carriers from flowing to the tunnel junction to recombine. However, when thicker p^+ and n^+ layers, with 20 s or longer deposition time, are used, V_{oc} drops significantly, from 2.31 V to 2.22 V. There are two possible reasons for this Voc drop. First, since the bandgap of a-Si decreases with increased doping, the effective bandgaps of the doped layers, p/p^+ and n/n^+, are reduced when the p^+ and n^+ layers are made thicker, resulting in a reduced built-in potential. Second, when the heavily doped layers are too thick, holes from p_1 (p_2) could fall into deep traps in p_1^+ (p_2^+) while electrons from n_2 (n_3) could fall into deep traps in n_2^+ (n_3^+); and these traps could be 50 Å apart, as in the case of GD854. These trapped charges could form a reversed electrical field at the p^+/n^+ interface, reducing the total voltage of the triple cell. These trapped charges also generate potential barriers at the p/p^+ and n/n^+ interfaces, hindering the flow of carriers toward the p^+/n^+ interface, resulting in reduced current, as reflected in the J_{sc} of GD854. The loss in FF in GD854 could have two contributions. First, it could be from these potential barriers indicated above. Second, the additional optical absorption by the thicker p_2^+/n_3^+ layers and p_1^+/n_2^+ would reduce the current of the middle and bottom component cells, respectively, causing the triple cell to be more limited in current, at the power point, by the middle or bottom cell which has poorer FF than the top component cell. This results in a drop in the overall triple-cell FF.

Fabrication of Triple-Junction a-Si Solar Cells

Incorporating optimized p^+/n^+ layers at the tunnel junctions, as well as other recent improvements related to our triple-cell fabrication including: 1) an improved intrinsic a-Si:H top cell i-layer made at low temperature and very high hydrogen dilution (see IV performance data of component cells in Table 3-2); 2) improved a-SiGe component cells using bandgap graded buffer layers [5] (See IV data in Table 3-2) ; 3) optimized nanocrystalline p-layer deposition conditions to reduce the band-edge offset at the p-i interfaces for component cells with different i-layer bandgaps [6]; and 4) a careful analysis of the light spectrum of our solar simulator and improved the current matching among component cells, we achieved the fabrication of a-Si/a-SiGe/a-SiGe triple cells with 12.7% initial efficiency. Figure 3-1 shows the IV curve of the 12.7% triple cell, GD585. The performance for the triple cell is V_{oc}=2.29V, J_{sc}=8.34 mA/cm^2, FF=66.5% and the initial efficiency is 12.7%.

Table 3-2 IV performance of top, middle and bottom component cells before and after 1000 hours of light soaking with 1 sun intensity at 50 ^{o}C.

Cell Number	Cell Type	Subs		Voc (V)	Jsc (mA/cm^2)	FF (%)	η (%)	Degradation (%)
Gd550-1	Top	SS	Initial	1.00	9.49	71.61	6.77	
			Stable	0.98	9.20	66.66	6.01	11.23
Gd572-2	Middle	BR	Initial	0.80	18.95	65.51	9.97	
			Stable	0.78	19.63	54.14	8.29	16.85
Gd575-2	Bottom	BR	Initial	0.62	22.85	60.96	8.57	
			Stable	0.62	22.94	52.44	7.41	13.54

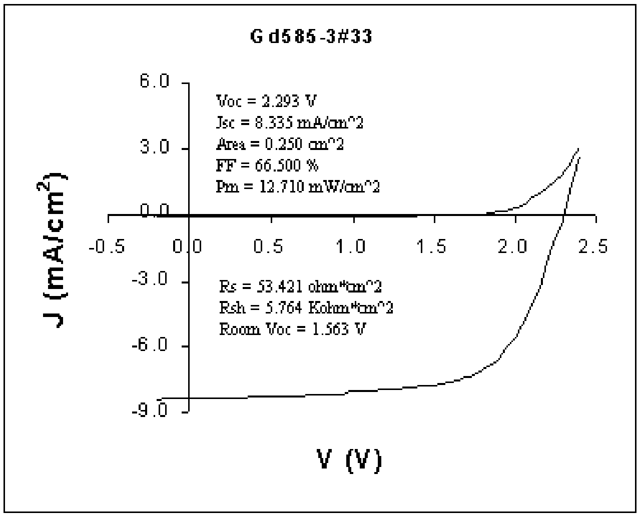

Figure 3-1 IV curve of a UT fabricated triple cell, showing 12.7% initial, active-area efficiency.

Figure 3-2 shows the quantum efficiency curves of the component cells in this triple cell. At the top of Figure 3-2, we show the calculated short circuit currents of the component cells under both UT simulator and the AM1.5 global spectrum. Since the Xenon lamp spectrum does not match exactly the AM1.5 global spectrum, different short circuit currents were obtained when being calculated using different spectrums. It should also be pointed out that the top cell current was calculated with wavelength longer than 370 nm. Therefore, the actual current should be larger than the current of shown in the figure for top cell by about 0.3 mA/cm^2 according to our estimate.

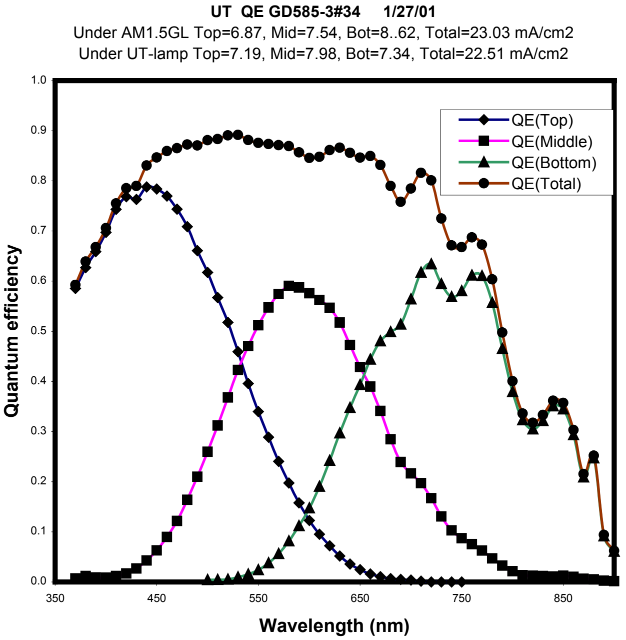

Figure 3-2 Quantum efficiency curve of 12.7% cell (GD585) showing the QE for top, middle and bottom cells. The figure also shows the short circuit current under UT simulator and AM1.5 spectrum.

Some triple cells fabricated at UT were sent to NREL for independent measurements. Table 3-3 shows the measurement for GD585 measured at NREL and UT, which agree with each other very well. The small difference in the J_{sc} and FF is because UT's simulator is slightly insufficient in the red, leading to a lower FF and a higher J_{sc} for a triple cell limited in the current by the top cell. The total-area η measured by NREL for GD585-3#33 is 11.8% (12.55% active-area), as shown in Figure 3-3.

Table 3-3 IV performance for triple-junction a-Si based solar cells measured at UT and NREL.

Cell#	V_{oc} (V)	I_{sc} (mA)	FF (%)	Active area (cm^2)	Active -area η (%)	Total area (cm^2)	Total -area η (%)	Measurem 't Lab
UT585-3#33	2.293	2.084	66.50	0.25	12.71			UT
UT585-3#22	2.286	2.046	66.35	0.25	12.41			UT
UT 585-3#33	2.3234	2.0591	67.17	0.256	12.55	0.272	11.81	NREL
UT 585-3#22	2.3191	2.0331	66.14	0.255	12.41	0.271	11.68	NREL

We have conducted light soaking stability tests for these UT fabricated triple-junction solar cells. After 1000 hours of one-sun light soaking at 50 ^{o}C, these triple cells degrade around 11-12% and show stable active-area efficiency above 10.5% with the highest stable efficiency (active area) at 10.7%, shown in Figure 3-4. The achievement of 10.7% stable efficiency is a significant improvement from our previously fabricated triple junction solar cells.

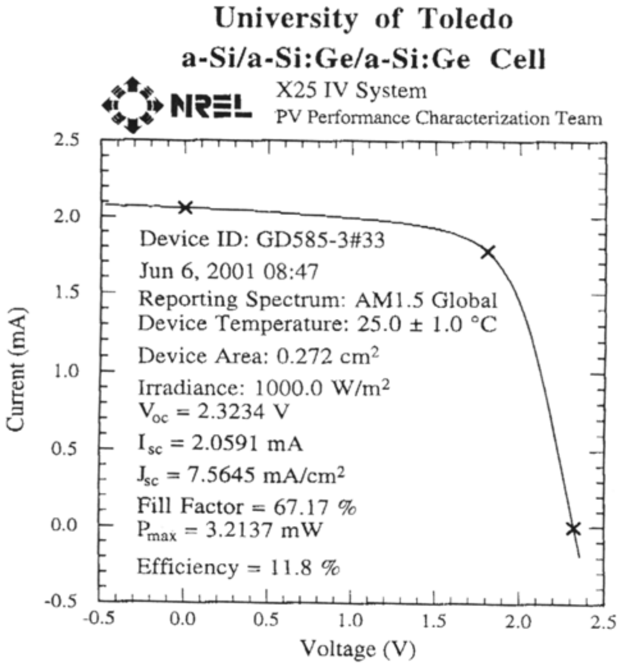

Figure 3-3 IV curve of GD585 measured at NREL, showing 11.8% initial, total-area efficiency.

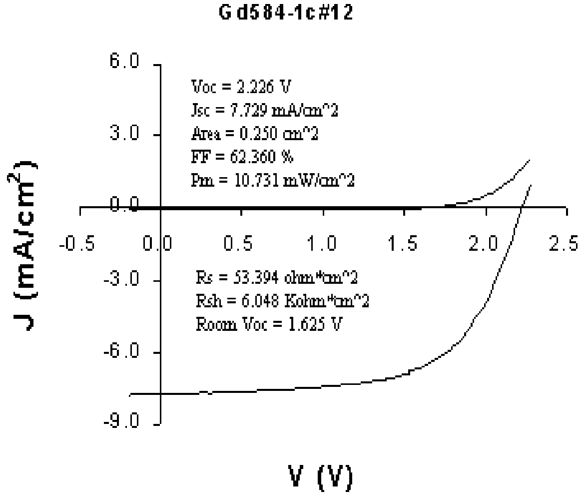

Figure 3-4. I-V curve of a triple cell showing 10.7% stable efficiency.

SUMMARY

The effect of heavily doped p^+/n^+ interface layers at the tunnel junction of triple-junction solar cells are studied. Preliminary results show that heavily doped thin interface layers could enhance the J_{sc} and FF of the triple cell. However, thicker interface layers (~4 nm or thicker) could result in significant reduction in Voc, Jsc and FF, possibly due to the formation of reversed electrical field at the tunnel junction and electrical potential barriers inside the doped layers.

Incorporating improved component cells and tunnel junctions into triple cell fabrication, we achieved triple-junction a-Si/a-SiGe/a-SiGe solar cells with 12.7% initial active-area efficiency. NREL measurements for these cells show 11.8% initial total-area efficiency (12.55% active-area efficiency). After 1000 hours of light soaking, these triple cells stabilized at efficiencies of 10.5-10.7%, with a degradation of 11-12%.

REFERENCES

1. J. Yang, A. Banerjee, and S. Guha, Appl. Phys. Lett. 70 2975 (1997).

2. A. Banerjee, J. Yang, T. Glatfelter, K. Hoffman and S. Guha, Appl. Phys. Lett. 64, 1517 (1994).

3. X. Deng, NREL Phase I Annual Subcontract Report, NREL/TP-411-20687, pp65-74. Available NTIS: Order No. DE9696000530 (Feb. 1996).

4. X.Deng, AIP Conf. Proc. 462, NCPV Photovoltaics Program Review, p.297 (1998).

5. X.B. Liao, J. Walker, and X. Deng, MRS Symp. Proc. **557**, 779 (1999).

6. X.B. Liao, W. Wang, and X. Deng, this Proceeding

Section 4 High Rate Deposition of Amorphous Silicon Films Using Hot-Wire CVD With Coil-Shaped Filament

Contributors: Henry S. Povolny and Xunming Deng

Abstract

To reduce the manufacturing cost for amorphous silicon (*a*-Si:H) based photovoltaics, it is important to deposit high-quality a-Si:H and related materials at high deposition rate. To this end, we designed and constructed a hot-wire deposition chamber with a coiled filament design and with multiple gas inlets. The process gas could be directed into the chamber through the filament coil and have maximum exposure to the high temperature filament surface. Using such a chamber design, we deposited *a*-Si:H films at high deposition rates up to 800 Å/s and dense, low-void a-Si:H at rates up to 240 Å/s.

1. Introduction

Considerable progress has been made in hydrogenated amorphous silicon (*a*-Si:H) based thin film photovoltaics during the recent years [1,2]. For high-efficiency solar cells, the *a*-Si:H layers in these devices have typically been deposited using RF Plasma Enhanced Chemical Vapor Deposition (PECVD). While RF PECVD produces cells with high efficiency, the deposition rates are generally low, around 1-5 Å/s. A number of alternative deposition techniques have been explored to deposit a-Si:H intrinsic layers at higher deposition rates. Using a very high frequency (VHF) PECVD process, high efficiency solar cell devices have been produced with a-Si:H intrinsic layers deposited at around 10 Å/s [3,4]. Hot-wire CVD (HWCVD) [5], also called Catalytic-CVD process [6], has been used to deposit a-Si:H based solar cells at higher deposition rates [7-9]. Although HWCVD-produced cells still show lower efficiency than PECVD-produced cell, the potential to deposit a-Si:H at higher rates makes HWCVD an attractive process for a-Si:H solar cell fabrication. In addition to photovoltaic application, a-Si:H is also used for other devices such as charged particle detectors [10,11]. In these devices, pin structures with i-layers thickness up to 10-20 μm are used to detect alpha particles or neutrons. Therefore, it is important to explore deposition processes that can be used to deposit a-Si:H films at high deposition rates. In this paper we report our study on the high-rate deposition of a-Si:H films using a HWCVD process employing a coiled filament design [12] and high flow rates.

2. Chamber Description

The Hot-Wire Chemical Vapor Deposition (HWCVD) chamber, shown in Figure 4-1, consists of a high vacuum chamber, a substrate holder, a coiled filament perpendicular to the substrate, two annular gas inlets near the substrate and one axial gas inlet directed through the filament coil, a gas confinement cup and an annular RF electrode for PECVD. The substrate holder, capable of holding a 10 cm by 10 cm substrate, is inverted over the gas confinement cup. Deposition was made on a variety of substrates including c-Si, quartz, 7059 glass, 1737 glass and stainless steel.

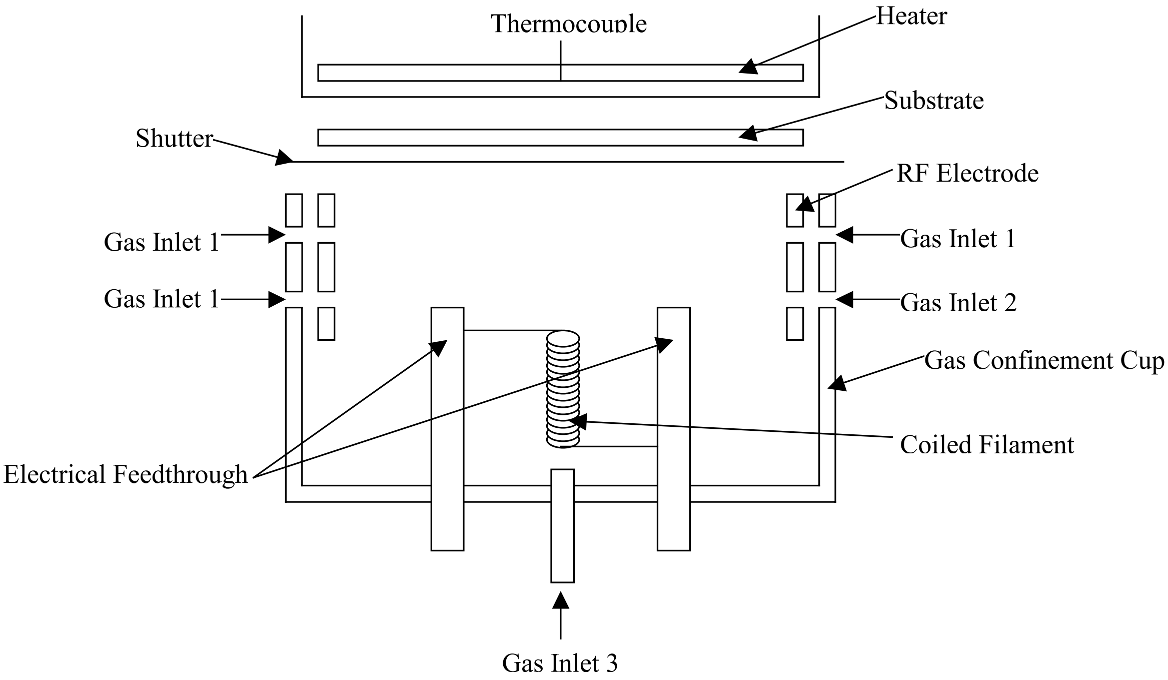

Figure 4-1 Schematic diagram of the Hot Wire CVD deposition chamber.

The filament coil is typically one meter of 0.75 mm diameter tungsten wire wound in a coil approximately 7 mm in diameter and 5 cm long with around 40 evenly spaced revolutions. Both 0.2 mm and 0.5 mm diameter tungsten wires were tried but did not support themselves at deposition temperatures. The filament is attached by a short, straight length of wire at the top and bottom to two vertical posts running parallel to the filament on either side approximately 2 cm away. The top of the filament can be positioned anywhere from 4.5 cm to 6.75 cm from the substrate though 5.7 cm was the distance used for this study. Temperature of the filament was calibrated using an optical pyrometer in vacuum and with hydrogen flow at various pressures. To maintain temperature of the 0.75 mm diameter tungsten wire at 2000 °C, currents between 29.5 amps and 31.5 amps were required depending on gas flow. Only a slight dependence on flow rate was noticed though higher pressures sometimes required current increases of 1 to 2 amps to maintain filament temperature.

Process pressures ranged from 7 mTorr to 200 mTorr for HWCVD and 500 mTorr for PECVD. Process gas flows ranged from a few sccm to 140 sccm. Deposition is fairly uniform over a 2 cm by 2 cm area in the center of the substrate area but falls off by 50% or less closer to the edge.

3. Experimental Details

A series of nine samples was prepared at high flow rates both with and without hydrogen dilution on a variety of substrates including 1737 glass, 7059 glass, quartz, crystalline silicon (c-Si) and stainless steel (SS). Pressure was 100 mTorr and the filament temperature T_{fil} was 2000 °C for all samples. Mixtures of Si_2H_6 and H_2 were used as the process gases. The substrate temperature T_{sub} ranged from 100 to 400 °C, which was the temperature of the substrates (actually measured at the position of the heater) before filament was turned on. The actual temperature of the substrate is expected to be higher due to filament heating. The other deposition conditions are summarized in Table 4-1. A surface profilometer was employed to measure film thickness. Transmission was measured to determine the thickness and the index of refraction from the interference fringes and band gap from the Tauc plot. Fourier Transform Infrared spectroscopy (FTIR) was performed to determine hydrogen content from the integrated area of the 640 cm^{-1} peak and bond preference from comparing the 2000 cm^{-1} (monohydride) and 2100 cm^{-1} (dihydride) peak heights. The microstructure factor, R*, the relative concentration of H in silicon dihydride and silicon polyhydride to the total H in the film, is calculated from the ratio of integrated absorption in the FTIR $[2100cm^{-1}]/([2100cm^{-1}]+[2000cm^{-1}])$. Lower R* suggests that the film is dense and has less micro voids. Electrical conductivity was measured to determine dark conductivity (σ_{dark}), photo conductivity (σ_{photo}) and the photo-to-dark conductivity ratio.

Table 4-1. Deposition conditions of a-Si:H films using HWCVD. All samples were deposited at 100 mTorr with a filament temperature of 2000 °C.

Sample	Si_2H_6 flow (sccm)	H_2 flow (sccm)	T_{sub} (°C)	Time (sec)	Thickness (μm)	Dep Rate (Å/s)	Sample ID
A1	105	0	100+	30	2.1	700	HW107
A2	105	0	200+	30	1.4	460	HW113
A3	105	0	300+	30	0.72	240	HW112
A4	105	0	400+	30	0.72	240	HW111
B2	105	100	200+	30	0.54	180	HW108
B3	105	100	300+	30	0.60	200	HW109
B4	105	100	400+	30	0.46	150	HW110
C	70	0	175+	120	2.4	200	HW105
D	140	0	100+	30	2.4	800	HW106

4. Results

Table 4-1 shows the deposition conditions of a series of nine samples deposited under different conditions. Samples A1, A2, A3 and A4 were deposited at substrate temperatures of 100, 200, 300 and 400 °C. All of these four samples were deposited with a Si_2H_6 flow of 105 sccm without hydrogen dilution. Samples B2, B3 and B4 were deposited at T_{sub} of 200, 300 and 400 °C while the flow of Si_2H_6 and H_2 were kept at 105 and 100 sccm respectively. Samples C and D were deposited with different Si_2H_6 flows, designed to see whether the deposition rate is limited by Si_2H_6 gas flows. All of the nine samples were deposited at a pressure of 100 mTorr and a filament temperature of 2000 °C. All samples were deposited with a deposition time of 30 seconds except Sample C, which was deposited in 120 seconds. The deposition time is controlled by a shutter. The total time taken in opening and closing the shutter is estimated to be less than 1.5 sec. The thickness in Table 4-1 is obtained using a surface profilometer, measured near the center of the film, directly above the coiled filament. From Table 4-1, we see that the deposition rate of the films ranges from 150 Å/s to 800 Å/s, depending on the Si_2H_6 gas flow and the substrate temperature.

The deposition uniformity is poor on the 10 cm by10 cm substrates due to the nature of the coiled filament and the fact that all of the process gases were directed into the chamber through the inlet adjacent to the filament. For example, profilometer measurements indicate that at a position 3 cm away from the center the film thickness drops approximately 30%. However, the thickness is fairly uniform within a 2 cm by 2 cm area near the center.

In Table 4-2, we summarize the results from UV-visible transmission spectroscopy, FTIR spectroscopy, and photo and dark conductivity measurement. The first column lists refractive indices *n* calculated by dividing *nd* from the transmission spectroscopy and *d* from the profilometer measurement. We did not rely soley on the thickness obtained from transmission measurements as there is a large variation in the index of refraction in this set of films and the films may not be highly uniform in thickness. Here *n* is the index in the long wavelength region. The optical bandgap E_g is calculated using Tauc plot $(\alpha h\nu)^{½} = B (h\nu – E_g)$. The bandgap for Samples A1 and D are approximate since Tauc plots do not yield straight lines. The hydrogen content (C_H) is calculated from the bending mode of the Si-H absorption (640 cm^{-1} peak) in the FTIR spectrum. We use a conversion factor of 2.3×10^{19} between H concentration and the integrated 640 cm^{-1} absorption peak [5] and a Si density of 5×10^{22} cm^{-3} to calculate C_H. For Samples A1 and D, the actual Si density could be lower so the C_H value could be higher than what is listed in Table 4-2. The Table also lists the film's microstructure factor R*, calculated from FTIR spectrum. In the last three columns of Table 4-2, we show the dark conductivity (σ_{dark}), photoconductivity (σ_{photo}), which is measured under 1 sun light intensity, as well as photosensitivity ($\sigma_{photo}/\sigma_{dark}$). σ_{photo} and σ_{dark} are measured using a coplanar geometry with painted silver paste electrodes.

Table 4-2. Properties of a-Si:H films deposited using HWCVD.

Sample	n	E_g(opt) (eV)	hydrogen (at %)	R* (2000vs.2100)	σ_{dark} (Ω^{-1}cm^{-1})	σ_{photo} (Ω^{-1}cm^{-1})	Photosensitivity
A1	1.9	~1.9	>10	1.0	<2x10^{-11}	1x10^{-10}	>5
A2	2.3	1.74	12	0.90	<2x10^{-11}	2x10^{-9}	>1x10^{2}
A3	3.6	1.63	10	0.17	4x10^{-10}	4x10^{-9}	9x10^{0}
A4	3.7	1.61	6	0.11	4x10^{-10}	5x10^{-9}	1x10^{1}
B2	3.6	1.78	19	0.50	<2x10^{-11}	2x10^{-8}	>1x10^{3}
B3	3.9	1.62	7	0.04	3x10^{-10}	1x10^{-8}	4x10^{1}
B4	4.3	1.63	3	0.05	2x10^{-10}	2x10^{-8}	1x10^{2}
C	3.6	1.63	8	0.36	2x10^{-11}	8x10^{-8}	4x10^{3}
D	1.6	~1.9	>8	1.0	3x10^{-11}	6x10^{-9}	2x10^{2}

For the four samples in series A that were deposited without H dilution, when T_{sub} increases from 100° to 400 °C, the deposition rate r_d drops from 700 to 240 Å/s, as we see from Table 4-1. However, as reflected in the increase in the index of refraction to ~3.7 and decrease in R*, at higher T_{sub}, the films are dense and with little micro voids. The bandgap drops down from ~1.9 eV to 1.61 eV, due to the drop in C_H in the film from 12 at.% or greater down to 6.0 at.% when T_{sub} is increased from 100° to 400 °C, since at higher T_{sub}, more H diffuses out of the film during the deposition, leaving less H inside. σ_{dark} increases with T_{sub}, consistent with reduced bandgap at higher T_{sub}. σ_{photo} increases with T_{sub}, partially due to the reduced bandgap and partially due to the improved structural properties. There is no obvious trend in the photosensitivity since σ_{dark} is below the limit of the electrometer currently used in our set up. Sample A1, although deposited at high deposition rate, contains high concentration of H in dihydride and/or polyhydride mode, indicating a porous film and is not of interest for photovoltaic applications.

With H dilution during the deposition, Samples in series B show a similar trend that at higher T_{sub} the films show higher n, lower bandgap, and less C_H but with lower R*. Comparing Samples B2 and A2, a moderate level of H dilution, with H_2:Si_2H_6=1:1.05, reduces the deposition rate but improves significantly the structural quality of the film, as reflected from the reduced R* and higher index of refraction. It contains more H than A2 and has a slightly higher bandgap. Comparing Samples B3 and B4 with Samples A3 and A4, a moderate level of H dilution does not change the bandgap or $\sigma_{dark,}$ but it reduces $C_{H,}$ reduces R* and increases σ_{photo} as well as the photosensitivity, and is therefore beneficial.

Sample A1, A2, C and D exhibit the effect of Si_2H_6 gas flow F as well as T_{sub}. At higher F and lower T_{sub} (Samples A1 and D), the deposition rate is high, up to 800 Å/s. However, the film is porous with an R*=1. At higher T_{sub} but lower F (Sample C), the film is denser and with low R*, but with lower $r_{d,}$ which is still much higher than the deposition rate typically reported in the literature, usually less than 50 Å/s. The photosensitivity is comparable among this set of films.

5. Discussions

We believe that the ability to grow films at high deposition rate is largely due to the highly efficient dissociation of gases at the filament due to the increased interaction time of the process gas with the filament. However, when the high flux of SiH_3 and other radicals arrive at the growth surface, SiH_3 radicals and H atoms do not have sufficient time to move around and find an appropriate site before the next radical arrives. Thus the non-ideal structure gets “frozen” and the material becomes porous. High temperature is needed so that the radicals on the surface can quickly move to favorable sites.

However, at these high temperatures hydrogen would diffuse out of the film at a correspondingly high rate. To maintain a high deposition rate and yet to keep H in the a-Si:H structure, we suggest to cool the substrate rapidly to below 250 °C after the completion of deposition at high T_{sub}. In this way high surface mobility can be maintained during the growth to promote dense, void free films, without losing hydrogen from the bulk due to effusion after the film is deposited.

6. Conclusion

Using a HWCVD process employing a coiled filament adjacent to the gas inlet, we deposited *a*-Si:H films at high deposition rates, in the range of 140 Å/s to 800 Å/s. The higher-rate samples are porous and contain H in mostly polyhydride bonding. At higher substrate temperature, *a*-Si:H films with low microstructure are deposited at a rate up to 240 Å/s. These films are dense but with relatively low H content. We suggest that dense a-Si:H films could be deposited at high rate (e.g., 800 Å/s) at a higher substrate temperature (e.g. 400 °C) but the substrates need to be cooled down rapidly from the growth temperature immediately after the deposition to prevent H from out effusion.

5. References

1. S. Guha, J. Yang, A. Banerjee, T. Glatfelter, K. Hoffman, S. Ovshinsky, M. Izu, H. Ovshinsky, X. Deng, Materials Research Society Symp. Proc. Vol. **336**, 645 (1994).
2. J. Yang, A. Banerjee, and S. Guha, Appl. Phys. Lett. **70**, 2977 (1997).
3. A. Shah, Dutta J, Wyrsch N, Prasad K, Curtins H, Finger F, Howling A, Hollenstein C, *Materials Research Society Symp. Proc. Vol.* **258**, 15 (1992).
4. X. Deng, Jones S, Liu T, Izu M, Ovshinsky S, *Proceedings of the 26th Photovoltaic Specialists Conference*, 591 (1997).
5. A. Mahan, Carapella J, Nelson B, Crandall R, Balberg I, *J. Appl . Phys*. **69**, 6728-6730 (1991).
6. H. Matsumura, *Jpn. J. Appl. Phys.* **25**, L949-951 (1986).
7. A. Mahan, Xu Y, Nelson B, Crandall R, Cohen J, Palinginis K, Gallagher A, *Appl. Phys. Lett.* **78**, 3788 (2001).
8. Q. Wang, E. Iwaniczko, J. Yang, K. Lord and S. Guha, MRS Proc. Vol. **664**, A7.5.1 (2001).
9. S. Bauer, B. Schroeder, W. Herbst and M. Lill, Proc. 2nd World Conf. on Photovoltaic Solar Energy Conversion, 363 (1998).
10. V. Perez-Mendez, J. Morel, S.N. Kaplan, and R.A. Street, Nuclear Instruments and Methods in Physics Research, **252**, 478 (1986).
11. D. Holcomb, A. Wintenberg, and X. Deng, "Pixelated neutron beam monitor development", in Proc. of International Workshop on Position-Sensitive Neutron Detectors--Status and Perspectives, June 2001, Hahn-Meitner-Institut, Berlin, Germany
12. M. Konagai, Kim W, Tasaki H, Hallerdt M, Takahashi K, *AIP Conf. Proc.* ***157***, 142-149 (1987).

Section 5 Phase Diagram for Deposition of Amorphous and Microcrystalline Silicon

Contributors: W. Wang, W. Du, X. Yang and X. Deng

Introduction

It is widely known that the deposition of amorphous and microcrystalline Si using PECVD and other thin film deposition processes depend on the hydrogen dilution of silicon containing gases (SiH_4 or Si_2H_6) in the gas phase. At lower hydrogen dilution, the film deposited is generally amorphous silicon, while at sufficiently higher hydrogen dilution, the film deposited becomes microcrystalline. For certain ranges of dilution, the film contains a mixed phases of amorphous and microcrystalline. However, the dilution level at which the phase transition from amorphous to microcrystalline occurs depends on other deposition conditions. For example, when a-Si film is thicker, it is more likely to form microcrystalline [1]. In this study, we explore the dependence of microcrystalline formation on the hydrogen dilution at different temperatures. This is important because when we want to deposit a-Si intrinsic layers for solar cells, we would like to deposit these materials near the onset of microcrystalline formation. Only if we know what is the transitioning dilution level for each temperature, we could deposit a-Si material with optimal dilution.

What is explored in this study are two dilution levels: R_{am}, the dilution level at which the transition between amorphous to mixed phase starts, and R_{mc}, the dilution level at which the mixed phase to pure microcrystalline phase starts. We investigate the dependence of R_{am} and R_{mc} on the substrate temperature.

The transition from a-Si to µc-Si depends not only on hydrogen dilution, it also depends on a variety of other factors, such as the film thickness and substrates. Since films for Raman measurement of microcrytalinity are usually deposited on glass and is thicker, the finding for R_{am} and R_{mc} may be different as in solar cell devices. To study the phase transition for application in solar cells, it is most applicable when these studies are done in real solar cell devices.

It has been reported [2] the open circuit voltage in single-junction a-Si solar cells is a sensitive measure of microcrystalline silicon formation. When the a-Si i-layer is deposited near the edge, i.e., protocrystalline, the open circuit voltage is the highest. When a mixed phase starts, the Voc starts to drop with increasing dilution. When the i-layer is dominated with microcrystalline, the Voc approaches 0.50 V. In this study, we use the open circuit voltage as an indirect measure of microcrystalline formation.

Experimental

Amorphous and microcrystalline n-i-p solar cells are deposited with a structure SS/n-i-p/ITO. All semiconductor layers are deposited using PECVD process. The deposition time of the i-layer is adjusted so that the i-layer thickness is approximately 120 nm, which is similar to the thickness of the i-layer as in a top component cell. The thickness of the device is calculated from the interference fringes in reflection spectra. The combined thickness of the doped layer is around 40 nm.

Forty-two nip deposition runs were made at dilution level R=$[H_2]/[Si_2H_6]$ of 25, 50, 100, 150, 175 and 200. The reading substrate temperature is set at 100, 150, 200, 250, 300, 350 and 400. The temperature range is selected to cover the temperature usually used to deposit a-Si and μc-Si while the dilution range is selected to cover the transition from amorphous to microcrystalline. Since the temperature is read from a location near the heater, away from the substrate, the actually temperature of the substrate is different. In Figure 5-1, we show the calibration of substrate temperature as a function of the reading temperature under different gas flow scenarios. From this calibration, substrate temperatures are obtained as 75, 115, 151, 187, 220, 260, 295 C. In fact, substrate temperatures quoted in our previous reports also need to be calibrated using Figure 5-1.

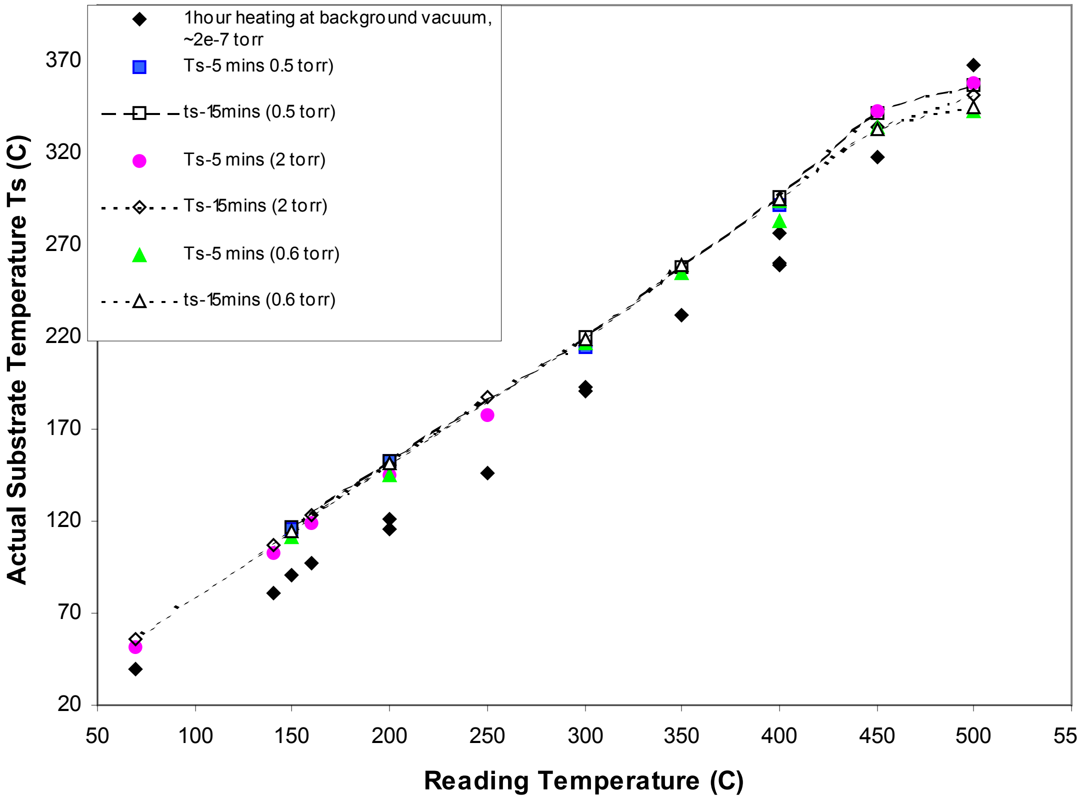

Figure 5-1. Calibration of actual substrate temperature from the reading temperature for UT's PECVD deposition system.

Results

Table 5-1 shows the PECVD solar cell fabrication runs conducted for this study. For each deposition run, four 2"x2" samples are deposited. On each 2"x2" sample, we fabricate an array of ITO contacts. Table 5-2 shows the thickness of the nip device on stainless steel measured using reflection interference fringes. This thickness includes the thickness of the doped layers, which is around 40 nm. Therefore, the thickness of the i-layer is around 120 nm. We show the thickness here since the transition from a-Si to uc-Si depends on the thickness for each dilution level. The effect of thickness was considered in the analysis. The deposition time for the i-layers deposited at a dilution levels R of 25, 50, 100, 150, 175 and 200 are 20, 30, 60, 90, 105 and 120 min, respective, except that GD783 was deposited in 127 min. From the deposition time and thickness, one calculate the deposition rate, as shown in Table 5-3.

Table 5-1 Single-junction a-Si solar cell devices fabricated to map out the deposition phase diagram in terms of substrate temperature and hydrogen dilution

Ts\R	25	50	100	150	175	200
295 ^{0}C	GD821	GD808	GD806	GD807	GD809	GD816
260 ^{0}C	GD788	GD782	GD779	GD792	GD810	GD789
220 ^{0}C	GD820	GD811	GD796	GD812	GD813	GD814
187 ^{0}C	GD819	GD804	GD780	GD794	GD805	GD815
151 ^{0}C	GD817	GD801	GD795	GD800	GD802	GD803
115 ^{0}C	GD818	GD797	GD781	GD791	GD793	GD783
75 ^{0}C	GD829	GD828	GD824	GD826	GD827	GD825

Table 5-2 Thickness of the nip layers for the 42 samples fabricated to map out the phase diagram. The thickness shown is in nm.

Ts\R	25	50	100	150	175	200
295 ^{0}C	158	171	164	159	164	176
260 ^{0}C	154	164	154	180	165	173
220 ^{0}C	171	158	166	158	181	160
187 ^{0}C	162	163	159	159	165	152
151 ^{0}C	168	156	153	140	169	148
115 ^{0}C	168	156	159	135	158	146
75 ^{0}C	157	148	145	154	158	156

Table 5-3 Growth rate, in A/s, of i-layers deposited under different conditions.

Ts\R	25	50	100	150	175	200
295 ^{0}C	0.98	0.73	0.35	0.22	0.20	0.19
260 ^{0}C	0.95	0.69	0.32	0.26	0.20	0.19
220 ^{0}C	1.10	0.66	0.35	0.22	0.22	0.17
187 ^{0}C	1.02	0.68	0.33	0.22	0.20	0.16
151 ^{0}C	1.06	0.65	0.31	0.19	0.21	0.15
115 ^{0}C	1.06	0.64	0.33	0.18	0.19	0.15
75 ^{0}C	0.97	0.60	0.29	0.21	0.19	0.15

Table 5-4 Open circuit voltage of the 42 samples fabricated to map out the phase diagram

Ts\R	25	50	100	150	175	200
295 ^{0}C	0.846	0.873	0.901	0.78	0.634	0.528
260 ^{0}C	0.91	0.921	0.924	0.77	0.572	0.52
220 ^{0}C	0.926	0.954	0.968	0.735	0.557	0.489
187 ^{0}C	0.948	0.979	0.989	0.783	0.538	0.48
151 ^{0}C	0.937	0.984	1.011	0.867	0.585	0.486
115 ^{0}C	0.929	0.976	1.014	0.814	0.542	---
75 ^{0}C	0.867	0.927	0.949	0.862	0.554	0.512

Table 5-4 shows the Voc for the set of devices. Each Voc value listed in Table 5-4 is the average of the Voc values from the ITO contacts that shows highest J-V performance on each sample. Sample GD783, deposited at Ts=115C and R=200, is shunted. Therefore, the Voc for this sample is discarded. As we can see from Table 5-4, the highest average Voc, 1.014 V, is obtained when the i-layer is deposited at around 120C with a H dilution of 100. The highest Voc is obtained near the transition region, at a dilution level right below that for microcrystalline formation. In Figure 5-2, we plot Voc for these devices as a function of R for each Ts. It is observed that 1) for all Ts, R=100 leads to the highest Voc; 2) at higher Ts, the drop in Voc when R is greater than 100 occurs more slowly with increasing R, while at lower Ts, the drop in Voc occurs rapidly; and 3) at higher R ~ 200, all samples show Voc around 0.5 V, indicating the i-layer contains large volume fraction of microcrystalline.

Based on the information in Table 5-4, we also generated a contour plot for Voc in the Ts—R graph. The contour plot shows that highest Voc is generated at R ~ 90 and Ts ~ 140 C.

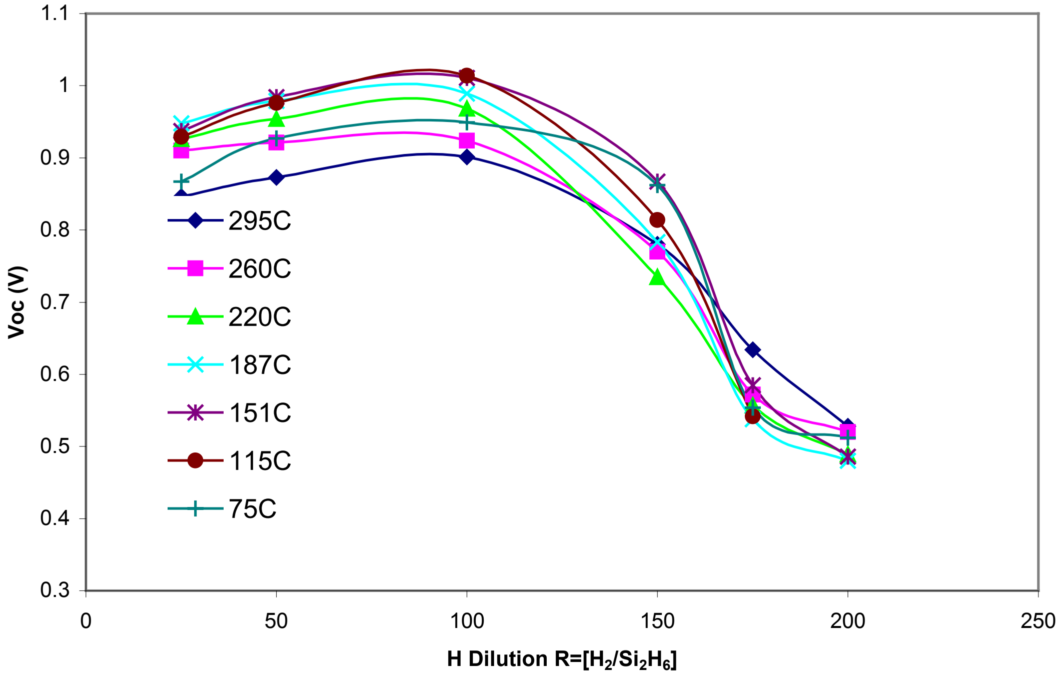

Figure 5-2 Voc of nip solar cells as a function of hydrogen dilution for different substrate temperatures

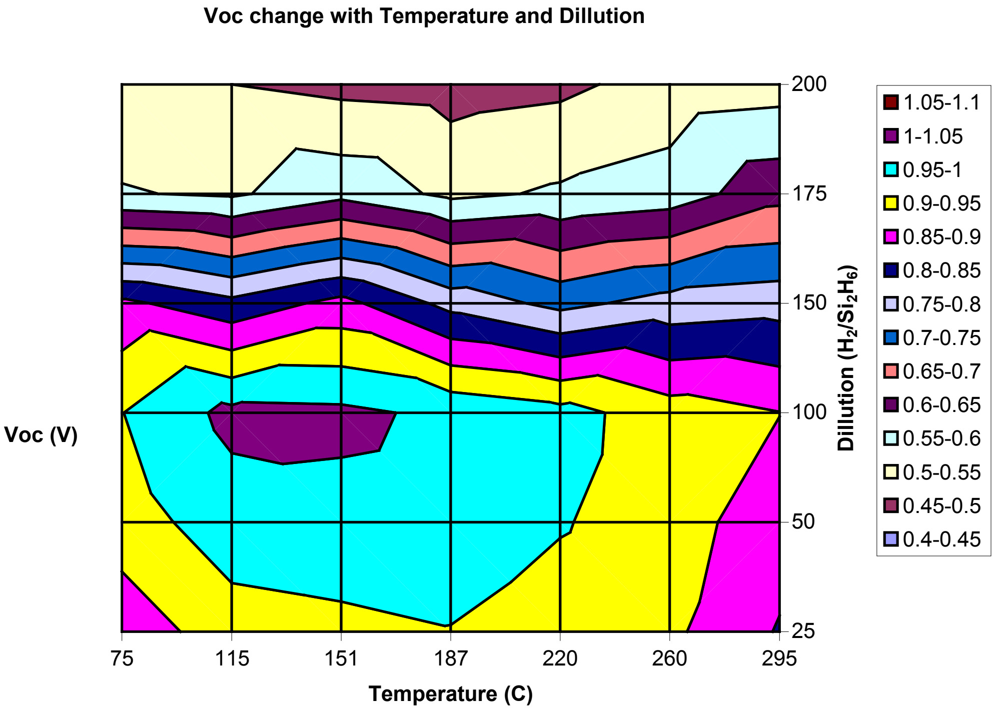

Figure 5-3 Contour plot of the Voc as a function of substrate temperature and H dilution

Discussions

Since the drop in Voc from above 0.9 V to 0.5 V with increasing R is due to the formation of microcrystalline phase in the bulk, we can use this study to generate deposition "phase diagram". The reason Voc starts to drop when R is increased beyond 100 is because small amount of microcrystals starts to form. From Figure 5-2, we estimate the dilution at which the Voc drops 10% from its maximum value and use this dilution, R_{am}, as the "phase boundary" between amorphous and mixed phases, as shown in Figure 5-4.

We then use the dilution R_{mc} at which the Voc drops down to 0.55V as the "phase boundary" between mixed phase and microcrystalline phase, since a significant amount of microcystalites must have been formed to drop Voc to around 0.50 V.

From Figure 5-2, we observe that R_{am} is lowest near 200 C and it increases at both higher Ts and lower Ts. For R_{mc}, it is somewhat flat at low Ts and it increase when Ts is increased beyond 200C. We think the reason that R_{am} is higher at low Ts, near 75 C, since at this Ts, the Si species stick to the surface easily and the material has a strong tendency to form polyhydride. Furthermore, these Si species may not land on a site that is desirable for microcrystalline Si formation and there is not enough surface mobility at this low temperature for these Si species to move around and find appropriate sites. Therefore, large amount of Si needs to be etched away from the surface through higher H dilution to form microcrystals. At higher Ts, again, we need to have more R to form microcrystalline Si. We think this is because at higher Ts, ~300C, there maybe less H coverage on the growth surface, resulting in reduced surface mobility during growth. Consequently, higher H is needed to form microcrystals.

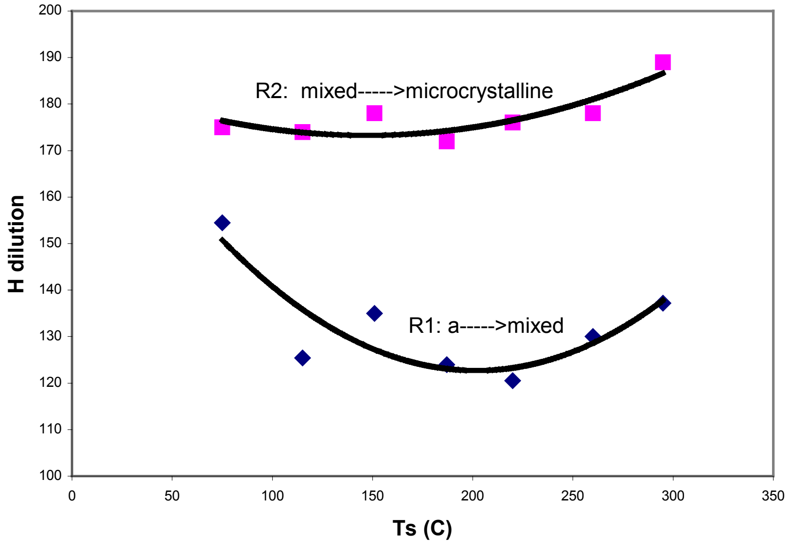

Figure 5-4 Phase diagram for the a-Si and microcrystalline growth in Ts-R plot.

Summary

Amorphous silicon solar cells are deposited at different substrate temperature Ts and with different H dilution R. We observed the change in Voc with increasing R for different Ts. It is found that the conditions near R~90 and Ts~140C are most desirable to lead to high Voc. We also generated a deposition "phase diagram" that maps out the formation of amorphous, microcrystalline and mixed phases. It is found that at Ts~200C, lowest R is needed to deposit microcrystalline Si. At both higher and lower Ts, we need higher R to deposit uc-Si.

Reference

[1] R. Collins et al. NREL a-Si team meeting. 2000.
[2] J. Yang et al, NREL a-Si team meeting. 2000.